Numerical study of effect of membrane properties on long-cycle performance of vanadium redox flow batteries

Zi Wei[1], N.A. Siddique[2a], Dong Liu[2b], Shambhavi Sakri[2c] and Fuqiang Liu[*1]

[1]*Department of Mechanical Engineering*
University of Massachusetts Lowell, Lowell, MA 01854, USA
[2]*Department of Materials Science and Engineering*
University of Texas at Arlington, Arlington, TX 76019, USA

Abstract. Fundamental understanding of vanadium ion transport and the detrimental effects of cross-contamination on vanadium redox flow battery (VRFB) performance is critical for developing low-cost, robust, and highly selective proton-conducting membranes for VRFBs. The objective of this work is to examine the effect of conductivity and diffusivity, two key membrane parameters, on long-cycle performance of a VRFB at different operating conditions using a transient 2D multi-component model. This single-channel model combines the transport of vanadium ions, chemical reactions between permeated ions, and electrochemical reactions. It has been discovered that membrane selecting criterion for long cycles depends critically on current density and operating voltage range of the cell. The conducted simulation work is also designed to study the synergistic effects of the membrane properties on dynamics of VRFBs as well as to provide general guidelines for future membrane material development.

Keywords: vanadium redox flow battery; CFD simulation; transient; crossover; membrane

1. Introduction

Vanadium redox flow batteries (VRFBs) are one of the most promising electrical storage devices. In a VRFB, electrical energy is stored in two soluble vanadium redox pairs with oxidation states of V-III and V-IV, respectively, in external electrolyte tanks. One of the key components of VRFBs is the membrane which prevents cross-mixing of the positive and negative half-cell electrolytes, while allowing the transport of charge-balancing ions. Vanadium ions permeation from one half-cell to the other reduces charge-discharge cell performance, efficiency, and capacity. Highly conductive and selective proton-conducting membranes are essential for efficient storage of electricity generated from, e.g., renewable energy sources, in order to create a more resilient energy infrastructure.

The in-cell performance of VRFBs is determined by a complex interplay between important membrane properties; however, membrane developers routinely rely solely upon out-of-cell measurement of membrane characteristics (Park and Kim 2015, Pezeshki, Tang *et al.* 2016). In VRFBs, membrane ionic conductivity and permeability of vanadium ions across the membrane,

---

∗Corresponding author, Professor, E-mail: Fuqiang_liu@uml.edu

and their synergistic effect, tend to be among the most significant factors to govern the storage efficiencies, including coulombic efficiency, voltage efficiency, and energy efficiency. More important, during long charge-discharge cycles of VRFBs the cross-contamination of vanadium ions creates an electrolyte capacity imbalance, i.e., a deviation in V-IV or V-III mole fractions which causes malfunction of the battery (Roznyatovskaya, Herr *et al*. 2016).

Numerical simulation is deemed as a powerful tool to study vanadium ion crossover and its detrimental effect, and provides information complementary to experimental investigation. So far transient numerical methods to study ion crossover and predict long-term performance of a VRFB have been limited to zero-dimensional models (Tang, Bao *et al*. 2011, Knehr and Kumbur 2012, Skyllas-Kazacos and Goh 2012, Agar, Knehr *et al*. 2013, Agar, Benjamin *et al*. 2014, Badrinarayanan, Zhao *et al*. 2014, Lei, Zhang *et al*. 2015, Boettcher, Agar *et al*. 2016) due to the computational simplicity. However, depending on the chemical structure of the membrane and operating conditions, a real VRFB could experience a significant vanadium ion concentration gradient along the flow channels that may make different contributions to the crossover resulting in capacity loss. This in combination with local electrolyte mass transport conditions could result in two-dimensional current distribution as demonstrated by (Clement, Aaron *et al*. 2016). Besides, most of the studies cited above treat the membrane as being selective only toward the transport of protons; the crossover of vanadium ions and its impact on the cell performance during long-term cycling are neglected. Therefore, to further shed lights on the effect of vanadium ion crossover, long-cycle simulation using either a two- or three-dimensional transient model is required.

In this study, we have developed a two-dimensional computational model based on the single-domain simulation which has been previously implemented to study fuel cells (Liu and Wang 2006, Ge, Xing *et al*. 2007) and batteries (Siddique and Liu 2010, Liu and Siddique 2011, Siddique, Salehi *et al*. 2012, Siddique, Allen *et al*. 2014). This work proposes a continuous electrochemical transport model coupled with chemical reactions between different vanadium species to investigate VRFB capacity loss and charge-discharge performance during extended-cycling operation. It is demonstrated that the present model enables a more realistic and comprehensive investigation of species crossover and could provide valuable guideline towards development of advanced membranes for next-generation VRFBs.

2. Numerical description

The model considers essential parts of the VRFBs including membrane and porous carbon electrodes, and the 2D computational domain is shown in Fig. 1. The battery channel is 2.24 cm long (x direction) with an active area of 5 cm^2.
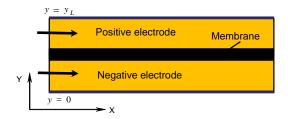

Fig. 1 Two-dimensional computational domain of a VRFB

2.1 Model assumptions

The model is based on the following assumptions:

1. The electrolyte flow is incompressible and laminar.
2. All elements are isothermal.
3. Water transport through the membrane is ignored.
4. Hydrogen and oxygen evolution reactions are neglected.
5. The dilute solution approximation is adopted for species transport.
6. The electrolyte density is constant and electrode properties are homogeneous.
7. Proton concentration is constant and uniform throughout the electrolyte.

2.2 Electrochemical reactions and transport characteristics

The electrochemical redox reactions occurring in the positive and negative half-cells are as follows

$$\text{VO}_2^+ + \text{e}^- + 2\text{H}^+ \xrightleftharpoons[\text{charge}]{\text{discharge}} \text{VO}^{2+} + \text{H}_2\text{O} \tag{1(a)}$$

$$\text{V}^{2+} \xrightleftharpoons[\text{charge}]{\text{discharge}} \text{V}^{3+} + \text{e}^- \tag{1(b)}$$

The transfer currents j for the positive and negative electrodes are described as (Boettcher, Agar *et al*. 2016)

$$j_1 = aFk_1 \left(c_{\text{VO}^{2+}} c_{\text{VO}_2^+} \right)^{0.5} \left[\exp\left(\frac{F}{2RT} \left(\phi_s - \phi_e - E_1^0 \right) \right) - \exp\left(-\frac{F}{2RT} \left(\phi_s - \phi_e - E_1^0 \right) \right) \right] \tag{2(a)}$$

$$j_2 = aFk_2 \left(c_{\text{V}^{2+}} c_{\text{V}^{3+}} \right)^{0.5} \left[\exp\left(\frac{F}{2RT} \left(\phi_s - \phi_e - E_2^0 \right) \right) - \exp\left(-\frac{F}{2RT} \left(\phi_s - \phi_e - E_2^0 \right) \right) \right] \tag{2(b)}$$

where E_0 is the equilibrium potential, ϕ_e the ionic potential, ϕ_s the electronic potential, a the specific active surface area of the porous electrodes, k_1 and k_2 the standard rate constants for the positive and negative electrodes, respectively. It should be noted that species migration is ignored here (Chen, Yeoh *et al*. 2014), because its contribution to species transport is not significant in the redox flow battery according to reference (You, Zhang *et al*. 2009).

The effective diffusion coefficients of species in the porous electrodes are calculated using the following equation, i.e.

$$D_i^{eff} = D_i \, \varepsilon^{1.5} \tag{3}$$

where ε is the porosity. The effective conductivity of the electrolyte is calculated by

$$\sigma_e^{eff} = \frac{F^2}{RT} \sum_i z_i^2 D_i^{eff} c_i \tag{4}$$

where F is the Faraday constant, z_i and c_i are the charge and concentration for species i, respectively.

The momentum equations for the porous electrodes account for the loss due to pressure drop as described by Darcy's law, which is inversely proportional to permeability (K) of the media. The permeability of the porous electrodes is described by the Carman-Kozeny equation as

$$K = \frac{d_f^2 \varepsilon^2}{16 k_{ck} (1 - \varepsilon)^2} \tag{5}$$

where d_f is the carbon fiber diameter and kck is the Carman-Kozeny constant, which depends on the type of porous media.

Compared to the diffusion coefficients of vanadium ions through Nafion membranes reported by (Sun, Chen *et al.* 2010) and many others, water can be considered to transport freely (Suresh, Scindia *et al.* 2005) across the membrane and therefore a balance of water between the anolyte and catholyte is easily maintained. Hence, we have ignored water transport in this study.

2.3 Vanadium ion crossover and relevant source terms

The following chemical reactions due to crossover of vanadium ions occur in both of the electrodes

$$V^{2+} + VO^{2+} + 2H^+ \rightarrow 2V^{3+} + H_2O \tag{6}$$

$$2V^{2+} + VO_2^+ + 4H^+ \rightarrow 3V^{3+} + 2H_2O \tag{7}$$

$$V^{3+} + VO_2^+ \rightarrow 2VO^{2+} \tag{8}$$

The chemical reactions (6)-(8) on both sides of the membrane consume vanadium ions at the reaction rates of

$$r_6 = k_{11} c_{V^{2+}} c_{VO^{2+}} \left[H^+ \right]^2 \tag{9}$$

$$r_7 = k_{22} \left[c_{V^{2+}} \right]^2 c_{VO_2^+} \left[H^+ \right]^4 \tag{10}$$

$$r_8 = k_{33} c_{V^{3+}} c_{VO_2^+} \tag{11}$$

where k_{11}, k_{22}, and k_{33} are the chemical reaction rate constants. These reactions may lead to a loss of columbic efficiency and appearance of concentration overpotential, which are detrimental to battery long-cycle performance.

2.4 Governing equations and source terms

The governing equations incorporating the aforementioned electrochemical transport equations and the source terms accounting for the species generation/consumption due to electrochemical reactions are listed in Table 1.

Table 1 Governing equations for the transport and electrochemical model

	Equations	Source Terms
Continuity	$\nabla \cdot \vec{u} = 0$	—
Momentum	$\dfrac{1}{\varepsilon^2} \nabla \cdot (\rho \vec{u}\vec{u}) = -\nabla p + \nabla \cdot \tau + S_u$	$S_u = -\dfrac{\mu}{K}\vec{u}$
V^{2+}	$\vec{u}\nabla c_{V^{2+}} - D_{V^{2+}}^{eff}\nabla^2 c_{V^{2+}} = S_{V^{2+}}$	$S_{V^{2+}} = -\dfrac{j_2}{F} - r_6 - 2\,r_7$ in negative electrode
V^{3+}	$\vec{u}\nabla c_{V^{3+}} - D_{V^{3+}}^{eff}\nabla^2 c_{V^{3+}} = S_{V^{3+}}$	$S_{V^{3+}} = \dfrac{j_2}{F} + 2\,r_6 + 3\,r_7$ in negative electrode
VO^{2+}	$\vec{u}\nabla c_{VO^{2+}} - D_{VO^{2+}}^{eff}\nabla^2 c_{VO^{2+}} = S_{VO^{2+}}$	$S_{VO^{2+}} = -\dfrac{j_1}{F} - r_6 + 2\,r_8$ in positive electrode
VO_2^+	$\vec{u}\nabla c_{VO_2^+} - D_{VO_2^+}^{eff}\nabla^2 c_{VO_2^+} = S_{VO_2^+}$	$S_{VO_2^+} = \dfrac{j_1}{F} - r_7 - r_8$ in positive electrode
Electron	$-\sigma_s^{eff}\nabla^2 \phi_s = S_s$	$S_s = -j$ in electrodes
Proton	$-\sigma_e^{eff}\nabla^2 \phi_e = S_e$	$S_e = j$ in electrodes

2.5 Boundary and initial conditions

The simulation is performed under galvanostatic operation and a constant current density is applied to the electrode/current collector interfaces, i.e.,
At $y=0$ (negative electrode/current collector interface)

$$\frac{\partial c_i}{\partial y} = 0, \quad \frac{\partial \phi_e}{\partial y} = 0, \quad -\sigma_s^{eff}\frac{\partial \phi_s}{\partial x} = -I \tag{12}$$

At $y=y_L$ (positive electrode/current collector interface)

$$\frac{\partial c_i}{\partial y} = 0, \quad \frac{\partial \phi_e}{\partial y} = 0, \quad -\sigma_s^{eff}\frac{\partial \phi_s}{\partial x} = I \tag{13}$$

At the left boundary, the reactants enter the cell with a prescribed velocity depending on the pumping rate. Concentration at the inlet boundary varies with time relying on the electrochemical reaction rate and cross-contamination of ions through the membane. The inlet concentrations are approximated using the following mass balance equations (Won, Oh *et al*. 2015) with assumption of instantaneous mixing in the electrolyte tank

$$c_{i,t}^{in} - c_{i,t-1}^{in} = \frac{Q}{V}\Delta t\left(c_{i,t-1}^{out} - c_{i,t-1}^{in}\right) \tag{14}$$

Where V is the volume of the electrolyte tank, Q is the electrolyte flow rate, the subscripts t and $t-1$ are the current and previous simulation time, Δt is the time step, and the superscripts *out* and *in* denote the outlet and inlet, respectively. Pressure outlet boundary conditions are applied to the right boundaries for the positive and negative half-cells.

The simulation was conducted by the SIMPLER algorithm in a commercial CFD software

Table 2 Parametric properties used in the simulation (You, Zhang *et al.* 2009, Al-Fetlawi, Shah *et al.* 2010, Sun, Chen *et al.* 2010)

Parameters	Value
Standard reaction rate constant, k_1 (m/s)	3.0×10^{-9}
Standard reaction rate constant, k_2 (m/s)	1.25×10^{-7}
Carbon fiber diameter, d_f (μm)	17.6
Porosity of carbon electrode, ε	0.83
Kozeny-Carman constant, k_{ck}	4.28
Electrode specific surface area, a (m^{-1})	12645.0
Equilibrium potential of the negative electrode, E_2^0	$E_2^0 = \dfrac{RT}{F} \cdot \ln\left(\dfrac{c_{V^{3+}}}{c_{V^{2+}}}\right) - 0.255$
Equilibrium potential of the positive electrode, E_1^0	$E_1^0 = \dfrac{RT}{F} \cdot \ln\left(\dfrac{c_{VO_2^+}}{c_{VO^{2+}}}\right) + 1.004$
Initial concentration of V^{2+}, $c_{V^{2+}}^0$ (mole/l)	0.1
Initial concentration of V^{3+}, $c_{V^{3+}}^0$ (mole/l)	0.9
Initial concentration of VO^{2+}, $c_{VO^{2+}}^0$ (mole/l)	0.9
Initial concentration of VO$_2^+$, $c_{VO_2^+}^o$ (mole/l)	0.1
Proton concentration, $c_{H^+}^0$ (mole/l)	3.0
Chemical reaction constant, k_{11}	8.0×10^{-7}
Chemical reaction constant, k_{22}	11.25×10^{-7}
Chemical reaction constant, k_{33}	8.0×10^{-7}

Fluent 6.3.26. User defined functions (UDF) are written to account for the diffusivity and source terms in different components.

3. Model validation

As a first step to validate the model, a 5-cm² VRFB cell was built and tested using graphitic carbon felt electrodes and Nafion 115 as the separator. 1 M vanadium sulfate in H$_2$SO$_4$ was initially used as the electrolytes for both the anolyte and catholyte. The cell was charged at a constant potential of 1.55 V to fully convert the vanadium species before cyclic tests at 20 mA/cm². The charge-discharge potential window is from 1.1 and 1.6 V. The simulation employed membrane properties reported by (Sun, Chen *et al.* 2010). Other parameters used in the simulation are listed in Table 2. Fig. 2 compares the simulated and experimental beginning-of-life charge-discharge curves. Very good agreement was found between the simulated and the experimental performance with only 3.9% average error in cell voltage during charge and discharge. Besides, the model precisely predicts the charge-discharge time and therefore battery
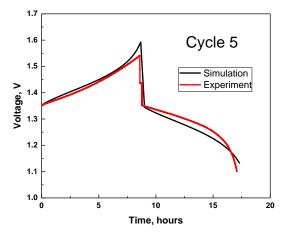
Fig. 2 Experimental and simulated beginning-of-life performance of a VRFB during Cycle #5. The charging/discharging current is 20 mA/cm^2

capacity, indicating legitimately reasonable assumption of the model and soundness of the parameters.

4. Results and discussions

In this work, membrane properties, including V^{2+}, V^{3+}, VO^{2+}, and VO_2^+ diffusivity (D_i) through the membrane and proton conductivity (σ), are systematically varied using a proportional factor (f, hereafter called "f factor") at 0.5, 1.0, and 1.5 with Nafion 115 as the reference, i.e., $D_i = f \cdot D_i^{NF115}$ and $\sigma = f \cdot \sigma^{NF115}$. The case of f=1.0 is for a VRFB with a Nafion 115 membrane; while other cases correspond to membranes with either proportionally increased or reduced ion diffusivity and conductivity. This simulation represents the actual dilemma in membrane design for VRFBs where membrane transport properties are intricately related and varying one parameter will trigger change of others. For example, membranes are normally not ion-selective and higher proton conductivity would naturally result in greater vanadium ion crossover rate.

Continuous charge-discharge cycles were simulated to study the impact of ion cross-contamination on long-term capacity and performance of the VRFB. Figs. 3(a)-(c) depict the simulated results using f factors of 0.5, 1.0, and 1.5, respectively. It is clear that all the VRFBs suffer from reduced capacity over time, especially for the case of f=1.5. This is represented by shortened time to charge the battery (and therefore discharge) due to ion cross-contamination. The reduced capacity is further illustrated in Fig. 4, where discharge capacity loss is compared at different f factors. The capacity is calculated using the discharge time and operating current density of 20 mA/cm^2. The VRFBs using different membranes initially display identical charge/discharge capacity at ca. 970 mAh, which continues decaying as the cycles proceed. As expected, the membranes with smaller diffusion coefficients of vanadium ions show lower rate of capacity fading. For example, the VRFB with f=0.5 loses its discharge capacity by 60% after 160 cycles and the one with f=1.5 reduces its capacity by 80% in 80 cycles. It should be noted that the simulated capacity decaying rate is relatively higher than what has been reported in reference
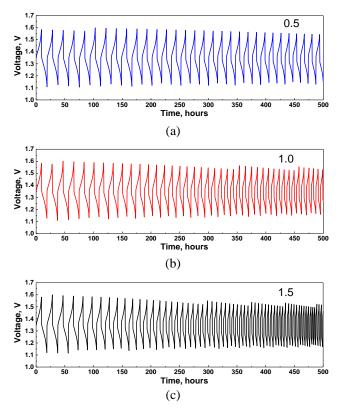
Fig. 3 Simulated continuous charge-discharge voltage profiles of a VRFB at 20mA/cm^2 with different membrane f factors: (a) 0.5, (b) 1.0, and (c) 1.5
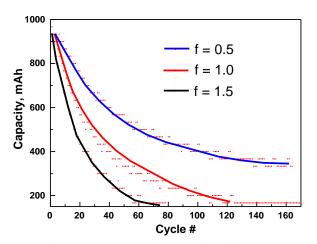

Fig. 4 VRFB capacity loss during cycles for membranes with different f factors. The charging and discharging current is 20 mA/cm^2

(Kim, Yan *et al.* 2010), owing to the fact that a more "leaky" membrane, i.e., Nafion 115, is studied herein in comparison to Nafion 117 or hydrocarbon membranes employed in reference
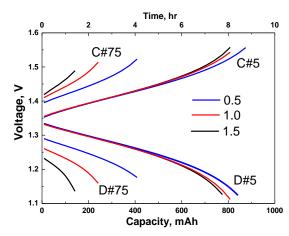
Fig. 5 Charge-discharge voltage profile of a VRFB with different membrane *f* factors during Cycle #5 and Cycle #75. The charging and discharging current is 20 mA/cm^2. "D" and "C" represent discharge and charge, respectively
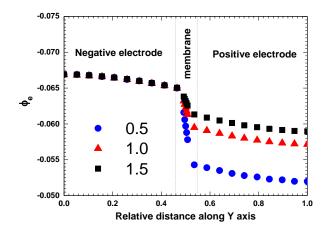

Fig. 6 Distribution of electrolyte potential as a function of the relative distance along Y axis for membranes with different membrane *f* factors. The curves are taken during battery charging of a VRFB at Cycle #5. The charging and discharging current is 20 mA/cm^2

(Kim, Yan *et al*. 2010). Besides, these results confirm that extended cycling test of flow batteries is essential for evaluating membranes as cross-contamination effect is accumulative on battery capacity.

In addition to the observed battery capacity fading, cross-contamination of vanadium species also leads to battery performance loss. Fig. 5 compares the charge-discharge curves for Cycle #5 and Cycle #75 using different membrane *f* factors. It is apparent that the f factors from 0.5 to 1.5 have marginal effect on battery charge-discharge performance during Cycle #5, except that the VRFB with *f*=0.5 slightly extends the charge/discharge time (therefore capacity). Further study on shown in Fig. 6 suggests that loss of ϕ_e is negligible in the studied range of conductivity values
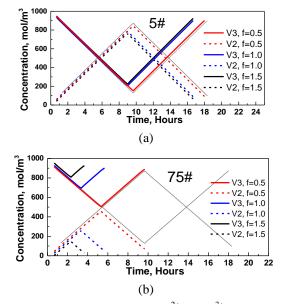
Fig. 7 Simulated variation of concentration profiles of V^{2+} and V^{3+} at the outlet during (a) Cycle #5 and (b) Cycle #75. The fine gray curves in both figures are for a case where zero vanadium ion diffusivity is assigned in simulation

as the membrane f factors increase from 0.5 to 1.5. For example, ϕ_e only drops ca. 15 mV for f=0.5 along the transverse direction of the battery (i.e., along Y axis), which is also justified by the low operating current density of the battery (20 mA/cm^2). In contrast, in Cycle #75 the effect of membrane f factor becomes significant in two folds: first, performance of the VRFBs is largely reduced due to cross-contamination of vanadium ions through "leaky" membranes; second, both the charge and discharge capacity reduces with increasing f factor.

To investigate the effect of ion crossover, variation of vanadium concentration at the outlet in the negative half-cell during Cycle #5 and Cycle #75 is compared with different f factors. In Fig. 7(a), compared to the gray curves representing an ideal case with no vanadium crossover (zero diffusion coefficient) through the membrane, all the three VRFBs display similar concentration variation and only those with higher f factors show slightly reduced V^{2+} and increased V^{3+} concentration, particularly during discharge. During Cycle #75 in Fig. 7(b), the observed change in vanadium concentration is further augmented and all the cells could not be fully charged. This is believed to be caused by cross-contamination of vanadium ions through the membranes, which continuously consumes, preferentially V^{2+} and VO_2^+ at the negative and positive half-cells, respectively. Vanadium concentration variation at the positive half-cell also displays similar trend and VO_2^+ concentration continues increasing in the positive half-cell as the cycling proceeds. The observed trend in variation of vanadium concentration in the VRFBs coincides with the recently experimental study conducted by (Luo, Wang *et al*. 2013). This cumulative ion crossover through the membrane creates imbalanced vanadium active species, but also the asymmetrical valence of vanadium ions in positive and negative electrolytes, leading to the notorious capacity fading over long charge–discharge cycling.

To further understand the effect of vanadium crossover, two additional cases are simulated. In
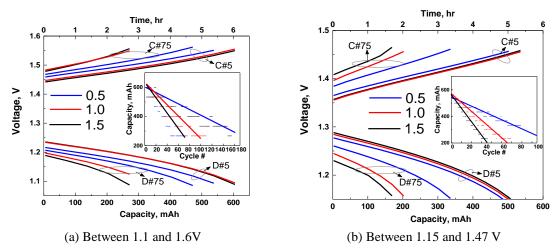
(a) Between 1.1 and 1.6V   (b) Between 1.15 and 1.47 V

Fig. 8 Simulated charge/discharge voltage profile of a VRFB with different membrane *f* factors at 40 mA/cm^2 during Cycle #5 and Cycle #75. Capacity fade during cycles for membranes with different *f* factors is shown in the inset

the first case, continuous charge and discharge of VRFBs were simulated at a higher current density, i.e., 40 mA/cm^2. The capacity fading and cell performance as a function of cycling numbers for three cases are compared in Fig. 8(a). Fig. 8(a) shows the simulated charge-discharge cell performance with different f factors during Cycle #5 and Cycle #75. In Cycle #5, different from what has been shown in Fig. 5, the case with *f*=1.5 yields the best charge-discharge cell performance, suggesting that membrane conductivity effect may outweigh that of ion permeation within the parameter range studied here. At around Cycle #15 (data not shown here), the higher membrane conductivity for the case with *f*=1.5 is counterbalanced by its higher ion diffusion rate in the membrane, and all three cases with different f factors display similar cell performance. Upon further increasing the cycles, difference between the charge and discharge potentials increases significantly for the membranes with larger *f* factors. In Cycle #75, the membrane with *f*=0.5 shows superior cell performance than the rest. In the inset of Fig. 8(a), the rate of VRFB discharge capacity fading is diminishing at a higher current density. The cell with *f*=0.5 loses its discharge capacity by 45% after 160 cycles (compared to 60% at 20 mA/cm^2 in Fig. 4) and the one with *f*=1.5 reduces its capacity by 58% in 70 cycles (compared to 80% at 20 mA/cm^2 in Fig. 4). This indicates that in the positive and negative electrodes, particularly near the membrane surface, more vanadium ions participate in electrochemical reactions at a higher current density; this leaves less of them available for crossing over the membrane. Therefore, the capacity loss becomes somewhat alleviated at higher operating current density. More important, it is noted that the three lines cross at around Cycle #15, where the combined membrane parameters act synergistically to yield a similar discharge capacity. In the second case, a narrower charge-discharge window between 1.15 and 1.47 V instead of between 1.1 and 1.6 V (Fig. 5) was simulated. The charging and discharging current is 20 mA/cm^2. In Fig. 8(b), capacity fading and cell performance as a function of cycling numbers for different membrane *f* factors are compared. Similar to the results in Fig. 8(a), battery cycling within a narrower potential window seems to reduce the effect of vanadium ion cross-contamination because of different membrane properties. The VRFB with *f*=1.5 displays the best beginning-of-life charge-discharge cell performance, and with increasing cycles the high proton

conductivity is counterbalanced by its higher ion diffusion rate through the membrane, resulting fast rate of capacity fading.

5. Conclusions

We present a continuous electrochemical transport model coupled with chemical reactions between different vanadium species to investigate VRFB capacity loss and charge-discharge performance during extended cycling. Different to conventional studies that focus on one or another membrane parameter, proportional variations in membrane diffusivity and conductivity, representing a practical problem in membrane design for VRFBs, at different current densities and potential windows are systematically investigated. It has been discovered that species diffusivity and membrane conductivity act synergistically in governing the overall cell performance and charge-discharge capacity. Low ion diffusivity in the membrane is beneficial for long cycles under low current density; however, it is could be overweight by better membrane conductivity to some extent. A crosspoint is observed where a high crossover rate could be compensated by better membrane conductivity, or vice versa. A higher current density was found to shift this crosspoint to longer cycles. Battery cycling within a narrower potential window seems to produce similar effects to those caused by a higher current density. The insights gained from this study could provide valuable guideline towards development of advanced membranes for next-generation VRFBs.

Acknowledgments

References

Agar, E., Benjamin, A., Dennison, C.R., Chen, D., Hickner, M.A. and Kumbur, E.C. (2014), "Reducing capacity fade in vanadium redox flow batteries by altering charging and discharging currents", *J. Pow. Sourc.*, **246**, 767-774.

Agar, E., Knehr, K.W., Chen, D., Hickner, M.A. and Kumbur, E.C. (2013), "Species transport mechanisms governing capacity loss in vanadium flow batteries: Comparing nafion® and sulfonated radel membranes", *Electrochim. Acta*, **98**, 66-74.

Al-Fetlawi, H., Shah, A.A. and Walsh, F.C. (2010), "Modelling the effects of oxygen evolution in the all-vanadium redox flow battery", *Electrochim. Acta*, **55**(9), 3192-3205.

Badrinarayanan, R., Zhao, J., Tseng, K.J. and Skyllas-Kazacos, M. (2014), "Extended dynamic model for ion diffusion in all-vanadium redox flow battery including the effects of temperature and bulk electrolyte transfer", *J. Pow. Sourc.*, **270**, 576-586.

Boettcher, P.A., Agar, E., Dennison, C.R. and Kumbur, E.C. (2016), "Modeling of ion crossover in vanadium redox flow batteries: A computationally-efficient lumped parameter approach for extended cycling", *J. Electrochem. Soc.*, **163**(1), A5244-A5252.

Chen, C.L., Yeoh, H.K. and Chakrabarti, M.H. (2014), "An enhancement to Vynnycky's model for the all-vanadium redox flow battery", *Electrochim. Acta*, **120**, 167-179.

Clement, J.T., Aaron, D.S. and Mench, M.M. (2016), "In situ localized current distribution measurements in

all-vanadium redox flow batteries", *J. Electrochem. Soc.*, **163**(1), A5220-A5228.

Ge, J., Xing, W., Xue, X., Liu, C., Lu, T. and Liao, J. (2007), "Controllable synthesis of pd nanocatalysts for direct formic acid fuel cell (DFAFC) application: From pd hollow nanospheres to pd nanoparticles", *J. Phys. Chem. C*, **111**(46), 17305-17310.

Kim, S., Yan, J., Schwenzer, B., Zhang, J., Li, L., Liu, J., Yang, Z. and Hickner, M.A. (2010), "Cycling performance and efficiency of sulfonated poly(sulfone) membranes in vanadium redox flow batteries", *Electrochem. Comm.*, **12**(11), 1650-1653.

Knehr, K.W. and Kumbur, E.C. (2012), "Role of convection and related effects on species crossover and capacity loss in vanadium redox flow batteries", *Electrochem. Comm.*, **23**, 76-79.

Lei, Y., Zhang, B.W., Bai, B.F. and Zhao, T.S. (2015), "A transient electrochemical model incorporating the donnan effect for all-vanadium redox flow batteries", *J. Pow. Sourc.*, **299**, 202-211.

Liu, F. and Siddique, N.A. (2011), "Microstructure reconstruction and direct evaluation of li-ion battery cathodes", *ECS Tran.*, **33**(24), 25-32.

Liu, F. and Wang, C.Y. (2006), "Optimization of cathode catalyst layer for direct methanol fuel cells: Part II: Computational modeling and design", *Electrochim. Acta*, **52**(3), 1409-1416.

Luo, Q., Li, L., Wang, W., Nie, Z., Wei, X., Li, B., Chen, B., Yang, Z. and Sprenkle, V. (2013), "Capacity decay and remediation of nafion-based all-vanadium redox flow batteries", *ChemSusChem*, **6**(2), 268-274.

Park, S.M. and Kim, H. (2015), "Hybrid membranes with low permeability for vanadium redox flow batteries using in situ sol-gel process", *Korean J. Chem. Eng.*, **32**(12), 2434-2442.

Pezeshki, A.M., Tang, Z.J., Fujimoto, C., Sun, C.N., Mench, M.M. and Zawodzinski, T.A. (2016), "Full cell study of diels alder poly(phenylene) anion and cation exchange membranes in vanadium redox flow batteries", *J. Electrochem. Soc.*, **163**(1), A5154-A5162.

Roznyatovskaya, N., Herr, T., Kuttinger, M., Fuhl, M., Noack, J., Pinkwart, K. and Tubke, J. (2016), "Detection of capacity imbalance in vanadium electrolyte and its electrochemical regeneration for all-vanadium redox-flow batteries", *J. Pow. Sourc.*, **302**, 79-83.

Siddique, N., Salehi, A. and Liu, F. (2012), "Stochastic reconstruction and electrical transport studies of porous cathode of li-ion batteries", *J. Pow. Sources*, **217**, 437-443.

Siddique, N.A., Allen, A.M., Mukherjee, P.P. and Liu, F. (2014), "Simulation of effect of interfacial lithium flux on miscibility gap in non-equilibrium phase transformation of LiFePO4 particles", *J. Pow. Sourc.*, **245**, 83-88.

Siddique, N.A. and Liu, F. (2010), "Process based reconstruction and simulation of a three-dimensional fuel cell catalyst layer", *Electrochim. Acta*, **55**(19), 5357-5366.

Skyllas-Kazacos, M. and Goh, L. (2012), "Modeling of vanadium ion diffusion across the ion exchange membrane in the vanadium redox battery", *J. Membrane Sci.*, **399-400**, 43-48.

Sun, C., Chen, J., Zhang, H., Han, X. and Luo, Q. (2010), "Investigations on transfer of water and vanadium ions across nafion membrane in an operating vanadium redox flow battery", *J. Pow. Sourc.*, **195**(3), 890-897.

Suresh, G., Scindia, Y.M., Pandey, A.K. and Goswami, A. (2005), "Self-diffusion coefficient of water in nafion-117 membrane with different monovalent counterions: A radiotracer study", *J. Membrane Sci.*, **250**(1-2), 39-45.

Tang, A., Bao, J. and Skyllas-Kazacos, M. (2011), "Dynamic modelling of the effects of ion diffusion and side reactions on the capacity loss for vanadium redox flow battery", *J. Pow. Sourc.*, **196**(24), 10737-10747.

Won, S., Oh, K. and Ju, H. (2015), "Numerical analysis of vanadium crossover effects in all-vanadium redox flow batteries", *Electrochim. Acta*, **177**, 310-320.

You, D., Zhang, H. and Chen, J. (2009), "A simple model for the vanadium redox battery", *Electrochim. Acta*, **54**(27), 6827-6836.

CC